Letter Vol. 6, No. 10 / October 2019 / Optica 1334

Picosecond pulses from a mid-infrared interband cascade laser

Johannes Hillbrand,[1,*] Maximilian Beiser,[1] Aaron Maxwell Andrews,[1] Hermann Detz,[2,3] Robert Weih,[4] Anne Schade,[5] Sven Höfling,[5,6] Gottfried Strasser,[1,2] and Benedikt Schwarz[1,7]

[1]Institute of Solid State Electronics, TU Wien, Vienna, Austria
[2]Center for Micro- and Nanostructures, TU Wien, Vienna, Austria
[3]Central European Institute of Technology, Brno University of Technology, Brno, Czech Republic
[4]Nanoplus Nanosystems and Technologies GmbH, 97218 Gerbrunn, Germany
[5]Technische Physik, Physikalisches Institut, University Würzburg, Am Hubland, 97074 Würzburg, Germany
[6]SUPA, School of Physics and Astronomy, University of St Andrews, St Andrews, KY16 9SS, UK
[7]e-mail: benedikt.schwarz@tuwien.ac.at
*Corresponding author: johannes.hillbrand@tuwien.ac.at

Received 20 June 2019; revised 23 August 2019; accepted 23 August 2019 (Doc. ID 370599); published 10 October 2019

The generation of mid-infrared pulses in monolithic and electrically pumped devices is of great interest for mobile spectroscopic instruments. The gain dynamics of interband cascade lasers (ICL) are promising for mode-locked operation at low threshold currents. Here, we present conclusive evidence for the generation of picosecond pulses in ICLs via active mode-locking. At small modulation power, the ICL operates in a linearly chirped frequency comb regime characterized by strong frequency modulation. Upon increasing the modulation amplitude, the chirp decreases until broad pulses are formed. Careful tuning of the modulation frequency minimizes the remaining chirp and leads to the generation of 3.2 ps pulses.

https://doi.org/10.1364/OPTICA.6.001334

Optical frequency combs (OFC) operating in the mid-infrared (MIR) spectral range are a powerful spectroscopic tool [1]. Measuring the molecular fingerprint in the MIR region allows the identification of chemical species the determination of their concentration. MIR frequency comb sources based on the nonlinear conversion of near-infrared mode-locked lasers [2,3] and microresonators [4] have reached a high level of maturity featuring octave spanning spectra [5]. Semiconductor laser OFCs [6] are advantageous in applications that require compactness and low power consumption. Quantum cascade laser (QCL) frequency combs [7,8] are among the most investigated technologies. However, gain bandwidth and dispersion [9,10] have so far limited their spectral bandwidth on the order of 100 cm^{-1}. One way to overcome this issue is spectral broadening in an external nonlinear fiber or waveguide. Recent results [11] have revealed, however, that the temporal output of QCLs is strongly chirped accompanied by the suppression of amplitude modulation. In fact, the ultrafast gain dynamics of QCLs are believed to be highly unfavorable for the formation of light pulses [12]. Previous attempts of mode-locking in monolithic QCLs were limited to cryogenic temperatures and low peak powers [13]. This makes nonlinear techniques for spectral broadening very inefficient. Further possible applications of short and intense mid-infrared pulses are numerous and promising, including nonlinear spectroscopy as well as optical ranging [14,15]. First results to enter the mid-infrared from shorter wavelengths were demonstrated using passively mode-locked GaSb-based type-I cascade diode lasers with 10 ps pulse duration around 3.25 μm [16].

Type-II interband cascade lasers (ICL) are an interesting alternative that already cover a major part of the mid-infrared up to 6 μm [17–19]. They combine the carrier injection and extraction scheme of QCLs with the advantages of an interband lasing transition. Hence, the upper-state lifetime of the optical transition in ICLs is on the order of 1 ns and thus significantly longer than the cavity round-trip time [18]. This enables low dissipation operation and has important consequences for mode-locking of ICLs. While the short upper-state lifetime of QCLs prevents the formation of short pulses, this issue is not present in ICLs. Furthermore, the ICL active material can be switched to absorption at the laser wavelength, which was shown by using ICLs as photodetectors at zero-bias [20]. Together with the fast carrier injection scheme, this allows the realization of efficient, high-speed modulators with cutoff frequencies of several gigahertz [21]. Hence, ICLs exhibit all required properties for efficient active mode-locking via modulation of the gain at the cavity round-trip frequency f_{rep} [22]. Recent efforts have been aimed at the generation of OFCs via passive mode-locking of ICLs. However, neither the interferometric autocorrelation nor multiheterodyne beating experiments showed the formation of pulses [23]. Instead, such passive ICL frequency combs are characterized by a continuous output intensity with a strong frequency modulation [21], similar to what was found in QCLs [8,11].

In this Letter, we report on the generation of picosecond pulses in two-section Fabry–Perot ICLs. The dry etched laser ridges are 6 μm wide and split into a 3520 μm long gain section and a 480 μm long modulation section [Fig. 1(a)]. The modulation section was designed to minimize parasitic capacitance for efficient RF injection. A 1.5 μm thick Si_3N_4 passivation layer was used for the modulation section while keeping its top contact area as small as possible. The passivation layer of the gain section is thinner (250 nm) to improve the thermal performance of the laser. The back facet of the device was high-reflection coated using Si_3N_4 and gold, while the front facet was left uncoated. The active region is comprised of six stages and operates at 3.85 μm (2600 cm^{-1}). At room temperature, the ICL emits up to 4.2 mW of optical power in continuous wave operation when both sections are biased homogeneously [Fig. 1(b)]. When the bias of the modulation section is set to 2.5 V additional loss is added to the cavity causing the threshold current density to increase and the maximum output power decreases to 1.9 mW. The injection of an RF signal at f_{rep} into the modulation section reduces the threshold by about 20%, showing that the laser is strongly influenced by the active modulation.

The characterization of the temporal output intensity of mid-infrared semiconductor lasers is challenging. Due to the high repetition rate and the relatively low average power, the peak power is expected to be too low for established nonlinear pulse characterization techniques [24]. Instead, we employ a linear phase-sensitive autocorrelation technique called "SWIFTS" [25]. This method uses a Fourier transform infrared (FTIR) spectrometer and a fast quantum well infrared photodetector (QWIP) to measure the amplitudes and phases of the beatings between adjacent laser modes (details in [25]). Hence, SWIFTS allows the reconstruction of both the temporal intensity and instantaneous frequency of the ICL frequency comb. Furthermore, recent experiments with a passively mode-locked quantum dot laser proved that SWIFTS and conventional intensity autocorrelation in a nonlinear crystal retrieve the same pulse width [26].

At 2.5 V bias of the modulation section, the laser generates a narrow beat note at the cavity round-trip frequency. This beat note results from the beating of adjacent cavity modes. Its narrow linewidth on the kHz level indicates that the cavity modes are phase-locked. To provide a stable reference for SWIFTS, we inject a weak RF signal at −2 dBm into the modulation section. Previous experiments showed that such a weak modulation is able to lock the frequency of the beat note and leaves the spectral phases of the free-running OFC unchanged [27]. The SWIFTS analysis of the ICL in this state [Fig. 2(a)] shows a 28 cm^{-1} wide intensity spectrum, which consists of several lobes. The SWIFTS spectrum has the same shape as the intensity spectrum [blue dots in Fig. 2(a)] over its entire span, which proves full phase-coherence and thus frequency comb operation. The intermodal difference phases $\Delta\phi$ retrieved from the SWIFTS data decrease linearly over a range of exactly 2π. This particular frequency comb state was found in QCLs operating at 8 μm [11], ICLs at 4 μm [21], and quantum dot lasers at 1.25 μm [26], and appears to be universal in semiconductor laser OFCs. Recent theoretical work attributes its origin to the interplay of dispersion and the Kerr effect in lasers with spatial hole burning [29]. Both SWIFTS interferograms [Fig. 2(a) right] have a local minimum at zero-path difference, which indicates the suppression of amplitude modulation [8]. Indeed, the reconstructed intensity [Fig. 2(b) top] does not show isolated pulses. In contrast, the instantaneous wavenumber is strongly modulated and linearly chirps through the entire spectrum within a cavity round-trip period.

In the following, we will investigate the influence of an increased modulation strength on the ICL frequency comb dynamics. Figure 3 shows the detailed SWIFTS analysis of the ICL for injection power levels from 6 to 36 dBm. The modulation frequency is altered slightly around f_{rep} to account for a small detuning of the laser round-trip frequency with temperature due to the high injection power. At 6 dBm [Fig. 3(a)], the ICL still operates in a similar OFC state as in Fig. 2(a) and the reconstructed time signal [Fig. 3(b)] does not show isolated pulses. When the injected power

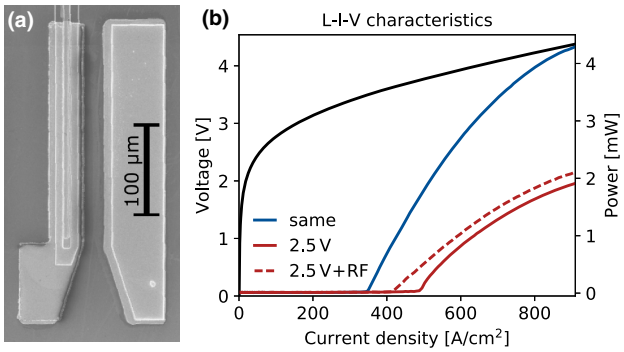

Fig. 1. (a) Scanning electron microscope picture of a 320 μm long modulation section of the ICL. The modulation section (left) and a ground contact (right) are optimized for RF injection via RF tips (Supplement 1, Fig. 1). A three-dimensional sketch of the entire device is illustrated in Supplement 1, Fig. 2. (b) Light-current-voltage (L-I-V) characteristics of the ICL at 15°C for a homogeneously biased laser (blue line) as well as for 2.5 V absorber bias with (dotted red line) and without (solid red line) RF modulation at $f_{rep} \approx 10.15$ GHz. The RF power is 31 dBm.

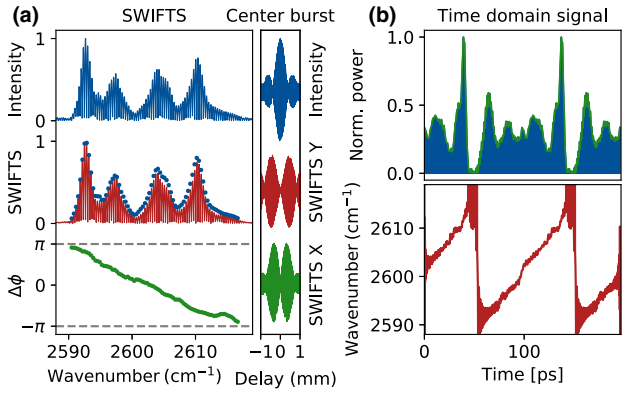

Fig. 2. (a) SWIFTS characterization of the ICL at −2 dBm injected RF power. The gain section is operated at 770 A/cm^2 and the modulation section at 2.5 V. The modulation section bias was optimized to obtain the narrowest beat note linewidth [28]. Blue line: intensity spectrum. Red line: SWIFTS spectrum. Blue dots: geometric average of neighboring modes of the intensity spectrum, which should be equal to the SWIFTS amplitudes in case of full phase coherence. Green dots: intermodal difference phases of adjacent comb lines. The right part shows a zoom-in on the center burst of the intensity and SWIFTS interferograms. (b) Reconstructed intensity and instantaneous wavenumber of the ICL frequency comb.

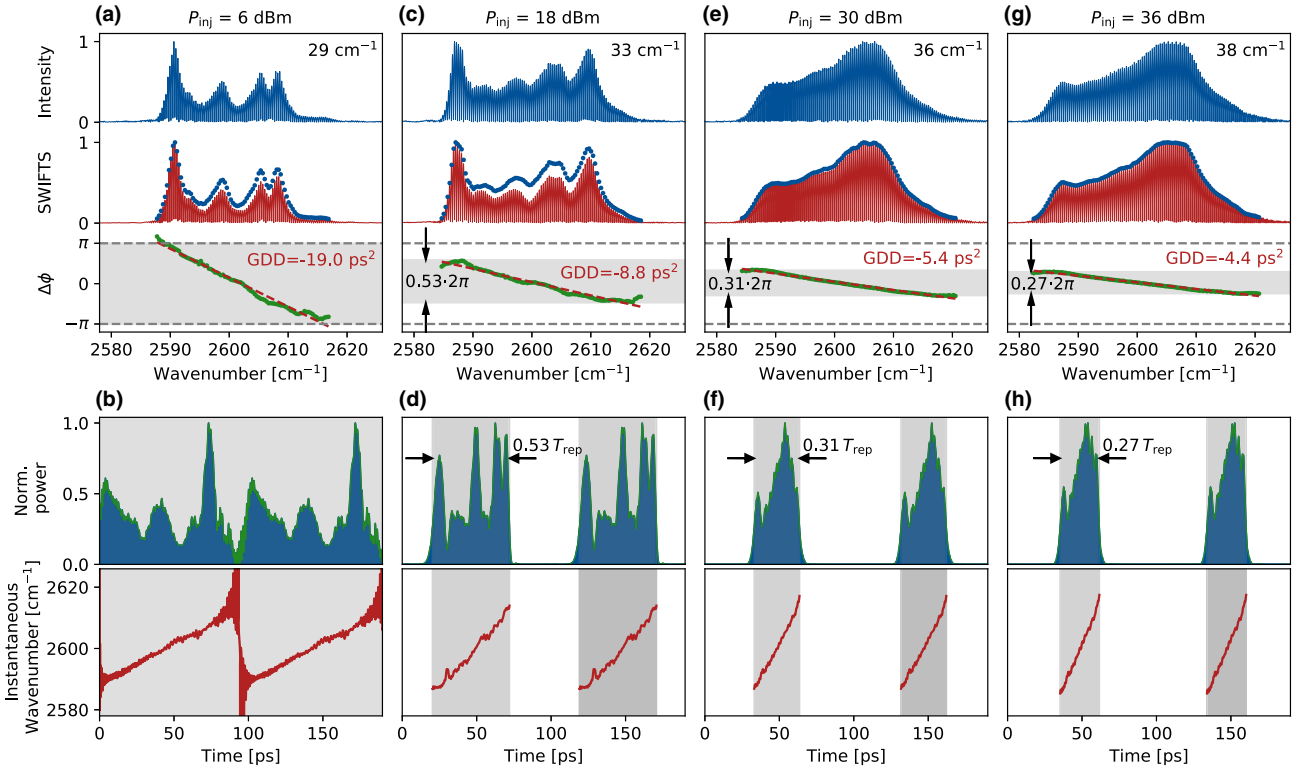

Fig. 3. SWIFTS analysis of the ICL frequency comb for 6 dBm (a), 18 dBm (c), 30 dBm (e), and 36 dBm (g) injected power. The wavenumber in the top right corner indicates the bandwidth of the spectrum. The gain section was operated at 800 A/cm^2 and the modulation section bias was 2.5 V. The GDD is deduced from the slope of the intermodal difference phases (red dotted line). (b), (d), (f), and (h) The corresponding reconstructed temporal intensity and instantaneous wavenumber. The shaded grey area indicates the phase range of $\Delta\phi$ and the duty cycle of the pulses. The time signal in (d) only shows the coherent part of the ICL output.

is further increased to 18 dBm [Fig. 3(c)], the spectral bandwidth grows to 33 cm^{-1} and the multiple lobes of the spectrum start to disappear. Interestingly, the SWIFTS spectrum shows that the ICL is not fully phase-locked in this transition state to the actively mode-locked regime. The intermodal difference phases still decrease linearly, but only cover the range of $0.53 \cdot 2\pi$. Since $\Delta\phi$ is directly proportional to the group delay with 2π corresponding to one cavity round trip, this means that the ICL emits pulses with roughly $0.53 \cdot 2\pi/2\pi \approx 53\%$ duty cycle. Indeed, the reconstructed time signal [Fig. 3(d)] shows broad and linearly chirped pulses. However, one should be careful when interpreting the reconstructed time signal of this partially coherent state because there could be an additional incoherent background. At 30 dBm, the spectrum consists of a single lobe spanning over 36 cm^{-1} [Fig. 3(e)]. The slope of $\Delta\phi$ decreases, which corresponds to a decrease of the group delay dispersion (GDD) to −5.4 ps^2 at 30 dBm compared to −19 ps^2 at 6 dBm. The reconstructed time signal [Fig. 3(f)] shows a train of isolated pulses with 27 ps full width at half maximum (FWHM). When the injected power is increased by another 6 dB, only a minor change in the shape of the spectrum and the GDD is observed [Fig. 3(g)].

Detuning the modulation frequency away from the round-trip frequency f_{rep} of the free-running laser is another knob to influence the temporal output of the laser. Figure 4(a) shows the SWIFTS characterization at 32 dBm injected power, while the modulation frequency is 15 MHz higher than f_{rep}. The spectrum consists of a single lobe spanning over 45 cm^{-1} and is fully coherent. Indeed, the intermodal difference phases do not show a linear chirp as in Figs. 3(a)–3(h) and occupy the phase range of only $0.13 \cdot 2\pi$. The reconstructed time signal [Fig. 4(b)] displays much shorter pulses than in Fig. 3(g) with a FWHM of 3.2 ps. The peak power is 114 mW, which is an enhancement of more than 40 with respect to the average power of 2.7 mW and proves that the energy can be efficiently stored by the gain medium over a round trip. The inset in Fig. 4(b) shows that the pulse is not transformation-limited with several smaller pulses arriving shortly after the first intense pulse. This is because the intermodal difference phases in Fig. 4(a) do not synchronize perfectly.

In conclusion, our results show that ICLs enable the generation of MIR pulses within a single semiconductor laser ridge. The weakly modulated ICL frequency comb operates in a regime characterized by a strong linear chirp, which was also found in QCLs and quantum dot lasers. When increasing the modulation amplitude, the laser spectrum broadens accompanied by the formation of broad and chirped pulses. By carefully tuning the modulation frequency away from the round-trip frequency of the free-running laser, the pulse duration decreases to 3.2 ps with a peak power enhancement of over 40. This illustrates the large potential of ICLs as a compact source for mid-infrared pulses. From the spectral bandwidth, one can assume that further optimization of the laser dispersion [30] (see Supplement 1, Fig. 3) and modulation section length will enable the generation of subpicosecond pulses [31].

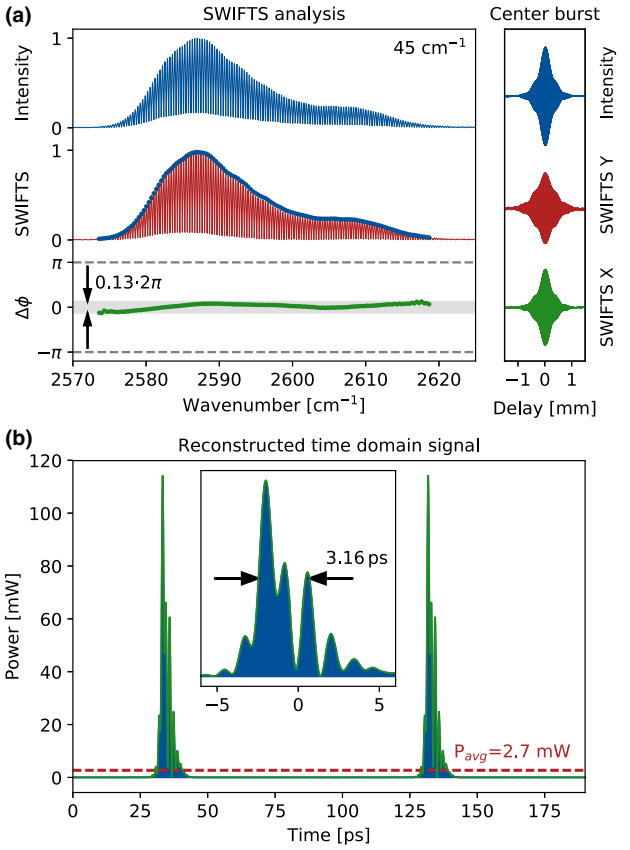

Fig. 4. (a) SWIFTS characterization for 920 A/cm^2 gain section current density and 3 V modulation section bias. The modulation power is 32 dBm and the modulation frequency is roughly 15 MHz higher than f_{rep}. In contrast to Fig. 2(a), both SWIFTS interferograms now have local maxima at zero delay of the FTIR mirrors, indicating strong amplitude modulation of the laser intensity. (b) Reconstructed time domain signal. Inset: Zoom on a single pulse, revealing a FWHM of 3.2 ps.

Funding. Austrian Science Fund (F4909-N23, P28914-N27, W1243); Österreichische Forschungsförderungsgesellschaft (ATMOSENSE, ERANet Photonic Sensing program, COMTERA-FFG 849614); European Science Foundation (ESF) (CZ.02.2.69/0.0/0.0/16_027/0008371); Air Force Office of Scientific Research (AFOSR FA9550-17-1-0340)

Acknowledgment. Johannes Hillbrand was supported by the city of Vienna. Hermann Detz was supported by the ESF. Aaron Maxwell Andrews was supported by the AFOSR.

See Supplement 1 for supporting content.

REFERENCES

1. A. Schliesser, N. Picqué, and T. W. Hänsch, Nat. Photonics **6**, 440 (2012).
2. F. Keilmann and S. Amarie, J. Infrared Millim. Terahertz Waves **33**, 479 (2012).
3. N. Leindecker, A. Marandi, R. L. Byer, K. L. Vodopyanov, J. Jiang, I. Hartl, M. Fermann, and P. G. Schunemann, Opt. Express **20**, 7046 (2012).
4. C. Y. Wang, T. Herr, P. Del'Haye, A. Schliesser, J. Hofer, R. Holzwarth, T. W. Hänsch, N. Picqué, and T. J. Kippenberg, Nat. Commun. **4**, 1345 (2013).
5. B. Kuyken, T. Ideguchi, S. Holzner, M. Yan, T. W. Hänsch, J. V. Campenhout, P. Verheyen, S. Coen, F. Leo, R. Baets, G. Roelkens, and N. Picqué, Nat. Commun. **6**, 6310 (2015).
6. G. Scalari, J. Faist, and N. Picqué, Appl. Phys. Lett. **114**, 150401 (2019).
7. J. Faist, F. Capasso, D. L. Sivco, C. Sirtori, A. L. Hutchinson, and A. Y. Cho, Science **264**, 553 (1994).
8. A. Hugi, G. Villares, S. Blaser, H. C. Liu, and J. Faist, Nature **492**, 229 (2012).
9. G. Villares, S. Riedi, J. Wolf, D. Kazakov, M. J. Süess, P. Jouy, M. Beck, and J. Faist, Optica **3**, 252 (2016).
10. J. Hillbrand, P. Jouy, M. Beck, and J. Faist, Opt. Lett. **43**, 1746 (2018).
11. M. Singleton, P. Jouy, M. Beck, and J. Faist, Optica **5**, 948 (2018).
12. A. Gordon, C. Y. Wang, L. Diehl, F. X. Kärtner, A. Belyanin, D. Bour, S. Corzine, G. Höfler, H. C. Liu, H. Schneider, T. Maier, M. Troccoli, J. Faist, and F. Capasso, Phys. Rev. A **77**, 053804 (2008).
13. C. Y. Wang, L. Kuznetsova, V. M. Gkortsas, L. Diehl, F. X. Kärtner, M. A. Belkin, A. Belyanin, X. Li, D. Ham, H. Schneider, P. Grant, C. Y. Song, S. Haffouz, Z. R. Wasilewski, H. Liu, and F. Capasso, Opt. Express **17**, 12929 (2009).
14. S. A. Meek, A. Hipke, G. Guelachvili, T. W. Hänsch, and N. Picqué, Opt. Lett. **43**, 162 (2018).
15. P. Trocha, M. Karpov, D. Ganin, M. H. P. Pfeiffer, A. Kordts, S. Wolf, J. Krockenberger, P. Marin-Palomo, C. Weimann, S. Randel, W. Freude, T. J. Kippenberg, and C. Koos, Science **359**, 887 (2018).
16. T. Feng, L. Shterengas, T. Hosoda, A. Belyanin, and G. Kipshidze, ACS Photon. **5**, 4978 (2018).
17. R. Q. Yang, Superlattices Microstruct. **17**, 77 (1995).
18. I. Vurgaftman, R. Weih, M. Kamp, J. R. Meyer, C. L. Canedy, C. S. Kim, M. Kim, W. W. Bewley, C. D. Merritt, J. Abell, and S. Höfling, J. Phys. D **48**, 123001 (2015).
19. C. L. Canedy, M. V. Warren, C. D. Merritt, W. W. Bewley, C. S. Kim, M. Kim, I. Vurgaftman, and J. R. Meyer, Proc. SPIE **10111**, 101110G (2017).
20. H. Lotfi, L. Li, S. M. S. Rassel, R. Q. Yang, C. J. Corrége, M. B. Johnson, P. R. Larson, and J. A. Gupta, Appl. Phys. Lett. **109**, 151111 (2016).
21. B. Schwarz, J. Hillbrand, M. Beiser, A. M. Andrews, G. Strasser, H. Detz, A. Schade, R. Weih, and S. Höfling, "A monolithic frequency comb platform based on interband cascade lasers and detectors," arXiv:1812.03879 (2018).
22. D. Kuizenga and A. Siegman, IEEE J. Quantum Electron. **6**, 694 (1970).
23. M. Bagheri, C. Frez, L. A. Sterczewski, I. Gruidin, M. Fradet, I. Vurgaftman, C. L. Canedy, W. W. Bewley, C. D. Merritt, C. S. Kim, M. Kim, and J. R. Meyer, Sci. Rep. **8**, 3322 (2018).
24. D. Kane and R. Trebino, IEEE J. Quantum Electron. **29**, 571 (1993).
25. D. Burghoff, Y. Yang, D. J. Hayton, J.-R. Gao, J. L. Reno, and Q. Hu, Opt. Express **23**, 1190 (2015).
26. J. Hillbrand, D. Auth, M. Piccardo, N. Opacak, G. Strasser, F. Capasso, S. Breuer, and B. Schwarz, "In-phase and anti-phase synchronization in a laser frequency comb," arXiv:1908.08504 (2019).
27. J. Hillbrand, A. M. Andrews, H. Detz, G. Strasser, and B. Schwarz, Nat. Photonics **13**, 101 (2019).
28. Y. Yang, D. Burghoff, J. Reno, and Q. Hu, Opt. Lett. **42**, 3888 (2017).
29. N. Opačak and B. Schwarz, "Theory of frequency modulated combs in lasers with spatial hole burning, dispersion and Kerr," arXiv:190513635 (2019).
30. D. Burghoff, N. Han, F. Kapsalidis, N. Henry, M. Beck, J. Khurgin, J. Faist, and Q. Hu, Appl. Phys. Lett. **115**, 021105 (2019).
31. J. Bowers, P. Morton, A. Mar, and S. Corzine, IEEE J. Quantum Electron. **25**, 1426 (1989).